Acoustic Modulation Enables Proton Detection With Nanodroplets at Body Temperature

Sophie V. Heymans, *Student Member, IEEE*, Gonzalo Collado-Lara, Marta Rovituso, Hendrik J. Vos, *Member, IEEE*, Jan D'hooge, *Member, IEEE*, Nico de Jong, *Member, IEEE*, and Koen Van Den Abeele

***Abstract*— Superheated nanodroplet (ND) vaporization by proton radiation was recently demonstrated, opening the door to ultrasound-based *in vivo* proton range verification. However, at body temperature and physiological pressures, perfluorobutane nanodroplets (PFB-NDs), which offer a good compromise between stability and radiation sensitivity, are not directly sensitive to primary protons. Instead, they are vaporized by infrequent secondary particles, which limits the precision for range verification. The radiation-induced vaporization threshold (i.e., sensitization threshold) can be reduced by lowering the pressure in the droplet such that ND vaporization by primary protons can occur. Here, we propose to use an acoustic field to modulate the pressure, intermittently lowering the proton sensitization threshold of PFB-NDs during the rarefactional phase of the ultrasound wave. Simultaneous proton irradiation and sonication with a 1.1 MHz focused transducer, using increasing peak negative pressures (PNPs), were applied on a dilution of PFB-NDs flowing in a tube, while vaporization was acoustically monitored with a linear array. Sensitization to primary protons was achieved at temperatures between 29 °C and 40 °C using acoustic PNPs of relatively low amplitude (from 800 to 200 kPa, respectively), while sonication alone did not lead to ND vaporization at those PNPs. Sensitization was also measured at the clinically relevant body temperature (i.e., 37 °C) using a PNP of 400 kPa. These findings confirm that acoustic modulation lowers the sensitization threshold of superheated NDs, enabling a direct proton response at body temperature.**

***Index Terms*— Acoustic droplet vaporization (ADV), acoustic modulation, nanodroplets (NDs), proton range verification, proton therapy, ultrasound contrast agents.**

Manuscript received March 27, 2022; accepted March 30, 2022. Date of publication April 6, 2022; date of current version May 26, 2022. This work was supported in part by the European Union's Horizon 2020 Research and Innovation Program under Grant 766456 ("AMPHORA") and in part by the Dutch Research Council under Grant NWA 1160.18.095. *(Sophie V. Heymans, Gonzalo Collado-Lara, Nico de Jong, and Koen Van Den Abeele contributed equally to this work.) (Corresponding author: Sophie V. Heymans.)*

Sophie V. Heymans was also with the Biomedical Engineering Group, Department of Cardiology, Erasmus University Medical Center (Erasmus MC), 3015 CN Rotterdam, The Netherlands. She is now with the Department of Physics, KU Leuven at Kortrijk, 8500 Kortrijk, Belgium, and also with the Department of Cardiovascular Sciences, KU Leuven, 3000 Leuven, Belgium (e-mail: sophie.heymans@kuleuven.be).

Gonzalo Collado-Lara is with the Biomedical Engineering Group, Department of Cardiology, Erasmus University Medical Center (Erasmus MC), 3015 CN Rotterdam, The Netherlands.

Marta Rovituso is with the Holland Proton Therapy Center, 2629 JH Delft, The Netherlands.

Hendrik J. Vos and Nico de Jong are with the Biomedical Engineering Group, Department of Cardiology, Erasmus University Medical Center (Erasmus MC), 3015 CN Rotterdam, The Netherlands, and also with the Department of Imaging Physics, TU Delft, 2628 CJ Delft, The Netherlands.

Jan D'hooge is with the Department of Cardiovascular Sciences, KU Leuven, 3000 Leuven, Belgium.

Koen Van Den Abeele is with the Department of Physics, KU Leuven at Kortrijk, 8500 Kortrijk, Belgium.

This article has supplementary downloadable material available at https://doi.org/10.1109/TUFFC.2022.3164805, provided by the authors.

Digital Object Identifier 10.1109/TUFFC.2022.3164805

I. Introduction

PROTON therapy is an advanced radiotherapy modality which has gained popularity in the past decade [1]. In contrast to high-energy photons, which traverse the entire patient's body, protons deliver most of their dose in a very localized region, called the Bragg peak, before abruptly stopping at a position known as the proton range [2]. The proton range can be tuned to correspond to the tumor location [3], thus enabling to better conform the dose distribution to the tumor and spare healthy tissues. However, the accuracy at which the range can be determined *in vivo* is limited by several sources of uncertainties, either with a physical or biological/anatomical origin [4], [5]. To prevent severe under- or over-dosages that may result from those uncertainties, safety margins, and suboptimal beam arrangements are currently adopted, compromising the tumor dose conformality [4], [6]. Therefore, *in vivo* range verification is critical to optimize the treatment precision and to allow proton therapy to reach its full potential.

The vaporization of superheated liquids by charged particles is a promising candidate for proton range verification. This technique was initially discovered in the 1950s in the context of bubble chambers [7], [8], and later expanded to superheated drop detectors [9], [10]. Recently, the concept was further extended to injectable superheated nanodroplets (NDs) and proposed as a new solution for ultrasound-based *in vivo* proton range verification [11]. In their liquid form, droplets are effectively invisible to ultrasound, but protons can induce ND vaporization through direct energy deposition, or by reactions that produce secondary charged particles (heavy recoil nuclei, alpha particles, etc.), turning them into echogenic microbubbles [11]. The stochastic distribution of ND vaporization events can be then acoustically measured, using either offline [12] or online [13] ultrasound imaging, and related to the spatial distribution of charged particles.

According to the thermal spike theory, charged particles trigger the vaporization of superheated liquids through homogeneous nucleation [7]. The energy deposited by the charged particle in the superheated liquid must exceed the energy required to create a gas embryo above a critical size, and must be deposited within a distance comparable to the diameter of the critical embryo. Mathematically, the condition can be written as

$$\left\langle \frac{dE}{dx} \right\rangle_{L_{\text{eff}}} \geq \frac{W_{\text{tot}}}{a R_c} \tag{1}$$

where $\langle dE/dx \rangle_{L_{\text{eff}}}$ is the ion track-averaged linear energy transfer (LET), W_{tot} is the critical embryo nucleation energy, R_c is the radius of a critical embryo, a is known as the nucleation parameter, and the product of a by R_c defines the effective length L_{eff}. W_{tot} and R_c can be calculated from the thermodynamic properties of the superheated liquid [10], [11]. The nucleation parameter, a, is an empirical constant for which values between 2 and 12 have been reported depending on the radiation type [10], [14], [15]. The right-hand side of equation (1) represents the sensitization threshold, i.e., the threshold which determines if a charged particle with a given LET can trigger droplet vaporization. The sensitization threshold depends on the degree of superheat of the liquid core [16], which is the temperature excess above the liquid boiling point, and which might be influenced by the droplet shell and size.

The degree of superheat can be tuned by varying the NDs internal temperature and pressure, and as it increases, NDs become sensitive to lower LET particles [14]. In a proton beam and at low degrees of superheat, only high LET secondary particles lead to ND vaporization [11], [12]. While the proton range can be indirectly inferred from the distribution of secondaries (using an approach similar to other range verification methods such as PET [17]–[19] and Prompt Gamma Imaging [20]–[22]), this method suffers from limitations. First, the fluence of high-LET secondary particles is two orders of magnitude lower than that of primary protons [23], requiring a higher droplet concentration to achieve the same number of vaporizations. Second, the process to infer the range suffers from uncertainties related to the nuclear reaction cross sections [4], [24]. Therefore, in order to obtain a precise and unambiguous measurement of the range, direct proton-induced ND vaporization is desirable.

One of the most common liquids used to produce superheated NDs is perfluorobutane (PFB, C_4F_{10}, boiling temperature of -2 °C at 1 atmosphere). Perfluorocarbons are biocompatible [25], and numerous studies have reported a good *in vivo* stability of coated Perfluorobutane nanodroplets (PFB-NDs) [26]–[29], making this liquid core a good candidate for clinical translation. Unfortunately, the degree of superheat of PFB is below the sensitization threshold for protons at the physiological temperature of 37 °C [12]. Previously, the degree of superheat of bubble chambers and superheated drop detectors was tuned by modifying the ambient temperature [30], [31], the static ambient pressure [32], or by using superheated liquids with different boiling temperatures [33], [34]. While the first two options are unfeasible in an *in vivo* application, the last option also suffers from several limitations. On the one hand, most of the superheated liquids used in *in vitro* detectors might not be biocompatible [35]. On the other hand, lower molecular weight perfluorocarbons, e.g., perfluoropropane (C_3F_8, boiling temperature of -37 °C): 1) have a reduced stability due to a faster dissolution of the droplet perfluorocarbon core into the surrounding liquid [26], [36]; and 2) are expected to lead to a large number of spontaneous vaporization events at physiological temperatures, as the degree of superheat will be closer to its limit [26], [36]–[38]. Thus, for *in vivo* range verification, a different approach to achieve direct vaporization of PFB-NDs by protons is preferred.

In the context of sono-photoacoustic imaging, the simultaneous use of ultrasound and pulsed laser radiation was shown to facilitate the vaporization of NDs coated with optical absorbers [39]–[41]. The vaporization threshold was reduced by the rarefactional phase of the acoustic wave compared to scenarios where ultrasound or pulsed laser illumination was used alone. Here, we propose a similar approach, in which an acoustic wave is used to dynamically increase and decrease the NDs degree of superheat during proton irradiation, reducing the energy required to trigger proton-induced vaporization during the rarefactional phase of the acoustic wave. Based on the thermal spike theory (1), which has only been validated for uncoated drops and hydrostatic pressure changes, a decrease of 73 kPa would enable proton-induced vaporization of PFB-NDs at 37 °C. We hypothesized that acoustic modulation with a relatively low frequency would have the same effect with similar pressure levels for coated NDs. This technique would enable direct *in vivo* proton range verification. In this study, we used an acoustic imaging platform to detect ND vaporization during proton irradiation in combination with a low-frequency acoustic modulation field, covering a range of acoustic amplitudes, at different temperatures. This allowed to demonstrate the feasibility of acoustic modulation and estimate the range of negative pressures which enable proton sensitization at each temperature, including the physiological case (i.e., 37 °C).

II. Materials and Methods

A. Nanodroplet Formulation

PFB-NDs with a polyvinyl alcohol shell (PVA-PFB) were prepared according to the protocol detailed in [42]. Briefly, an empty glass vial sealed with a rubber cap was immersed in liquid nitrogen, and gaseous PFB was injected into the vial. The PFB quickly cooled and condensed in the closed vial. Subsequently, 5 mL of a PVA and $NaIO_4$ (2% mol/mol) solution in milli-Q water (2% w/v) were injected into the closed vial, followed by sonication in an ice-cold ultrasonic bath (Emi30, EMAG, Waldorf, Germany) for 15 min at 100% power to encapsulate the liquid PFB in PVA shells. After storage at 4 °C for 1 h, the shell crosslinking was completed and the NDs were washed in a two-step centrifugation process: after a first centrifugation at 1000 g for 5 min, the supernatant was re-centrifuged at 2600 g for 7 min. Both pellets were then recombined and redispersed in 5 mL of Milli-Q water, yielding

a droplet concentration in the range 5–50 mM (PFB in water concentration measured with Nuclear Magnetic Resonance spectroscopy). The radiation sensitivity of this ND formulation has been demonstrated in previous studies [12], [13], [42]. The intensity-weighted mean diameter of this ND formulation, measured by Dynamic Light Scattering, is 799 ± 25 nm, with a polydispersity index of 0.3 [12] (see Fig. S1). NDs were stored at 4 °C and used within four days post preparation.

B. Acoustic Modulation Transducer

In order to achieve a quasi-static pressure modulation with respect to the time scales of radiation-induced vaporization, a 1.1-MHz acoustic frequency was used. The quarter period of MHz waves is several orders of magnitude longer than the time necessary for an ion to nucleate a critical embryo, which was estimated to be in the order of tens of picoseconds [7]. This low frequency also ensures a relatively uniform pressure distribution within the droplet, whereas higher frequencies would lead to unwanted effects such as droplet resonance [43] or acoustic focusing [44]. A custom-made high-intensity focused transducer was used (center frequency 1.1 MHz), built from a spherically focused PZT element (48 mm, Meggit Ferroperm, Coventry, U.K.) and air-backed to ensure a high transmission efficiency. The steady-state pressure field (see Fig. S2) and peak negative pressure (PNP) at focus were characterized using a calibrated needle hydrophone (0.2 mm, Precision Acoustics, Dorchester, U.K.) while driving the transducer with a 30-cycles sine wave. The acoustic focus was located at 48 mm, and the −6-dB length and width at focus were 15 and 1.8 mm, respectively.

C. Experimental Setup

Proton irradiation experiments were carried out at the research beam line of the Holland Proton Therapy Center (Delft, The Netherlands). The beam line provides a continuous horizontal pencil beam, with clinical settings (proton energies ranging from 70 to 250 MeV and beam intensities from 1 to 800 nA at beam extraction). A clinically relevant beam energy of 158 MeV was used for the current experiments (corresponding to a range in water of 17 cm). A water tank equipped with resistive heaters and a temperature control unit was positioned with its entrance wall located at the isocenter (i.e., the reference point in the proton beam path) (see Fig. 1(a)). The irradiation target was a cellulose tube (6-mm diameter, 75-μm wall thickness, Serva Electrophoresis GmbH, Heidelberg, Germany), in which an ND solution was flowing. The tube was positioned vertically and perpendicular to the proton beam direction. Both ends of the cellulose tube were connected to smaller tubes (1.5-mm-inner diameter), one of them connected the cellulose tube with a syringe pump (inlet), while the other served as an outlet. To ensure inflation of the cellulose tube, a moderate overpressure (0.36 bar) was achieved by connecting a 30G needle to the tube outlet. In order to avoid variations in overpressure with temperature, the outlet of the tube was cooled down in a water reservoir at room temperature (not drawn in Fig. 1(a)).

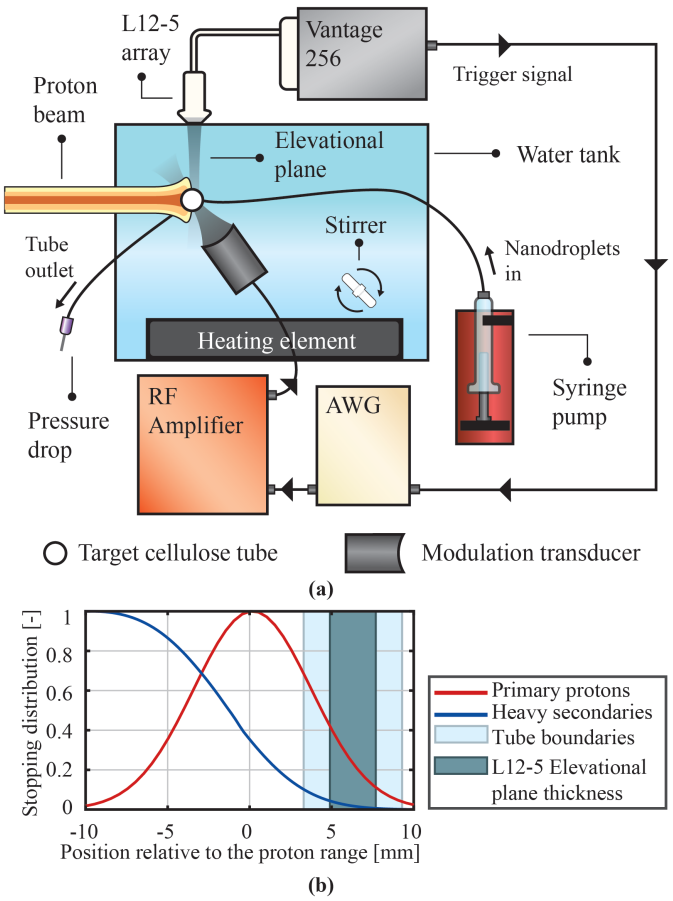

Fig. 1. (a) Schematic of the setup (top view). The proton beam, modulation transducer, and linear array were co-aligned to the target tube in which NDs were flowing. (b) Position of the cellulose tube with respect to the stopping distribution of charged particles. The tube area is shown together with the −6-dB elevational plane thickness of the L12-5 probe.

The modulation transducer was located inside the water tank, at the same height as the proton beam axis, and focused at the center of the cellulose tube. The transducer was driven with signals generated by an AWG (ww2571a, Tabor Electronics, Nesher, Israel) and amplified by 53 dB (150A100B, Amplifier Research, Sourdeton, PA, USA). An L12-5 linear array was used to image the tube and capture ND vaporization events. The linear array was fixed outside the water tank and connected to a Vantage 256 system (Verasonics, Kirkland, WA, USA). Acoustic coupling was ensured by a 20-μm-thin polyester window attached to the wall of the water tank. The linear array was positioned parallel to the tube, providing a long axis cross-sectional image in the flow direction. In order to co-align the modulation transducer and the linear array, the tube was temporarily replaced with a 1-mm-diameter steel rod fixed at the location corresponding to the center of the tube and the pulse-echo signals of both acoustic probes were maximized.

In order to reduce unwanted vaporization events owing to high-LET particles, the center of the tube was positioned at the wake of the proton stopping distribution (see Fig. 1(b)). Indeed, the fluence of high-LET secondaries drops proximal

to the primary proton fluence due to the Coulomb barrier [45]. While this choice of tube position also led to a reduction in the number of stopping protons, the ratio of primary protons to secondary particles increased by one order of magnitude. The exact position of the tube with respect to the proton range was measured independently using the technique presented in [13], and the tube was found to be located 6.1 mm behind the position at which 50% of the primary protons have stopped (i.e., the proton range).

D. Acoustic Modulation Experiment

ND dilutions were prepared by mixing 800 μL of native suspension with 60 mL of Milli-Q water (estimated concentration in the tube of 60–700 μM). The dilution was driven from the syringe directly through the tube at 1.8 mL/min using a syringe pump (AL-1000, World Precision Instruments, LLC, Sarasota, FL, USA) and irradiated with a proton flux of 2.22×10^8 protons/s at the center of the tube (400-nA beam current at extraction). The water tank was heated to 50 °C and allowed to reach gas equilibrium overnight. During the experiments, the heating system was turned off and proton-induced ND vaporization was monitored during cooling down, while a magnetic stirrer kept the temperature homogeneous inside the tank. A thermal IR camera (i7, Teledyne FLIR, Wilsonville, OR, USA) facing the cellulose tube recorded the temperature. The ND solution was refreshed every 20–30 min. Thus, measurements were performed between 50 °C and 29 °C (including 37 °C). At 50 °C, 43 °C, 39 °C, and 35 °C, the droplet dilution in the syringe was renewed.

Two different sets of recordings were acquired, depending on whether the temperature was above or below the proton sensitization threshold for the NDs used:

1) Sensitivity to Protons at Ambient Conditions: First, the temperature at which the droplets lost sensitivity to protons at ambient pressure was determined. Acoustic recordings were performed during proton irradiation, without acoustic modulation, at different temperatures during cooling down of the water tank.

2) Acoustically-Induced Sensitivity to Protons: Once a drastic decrease of the number of vaporization events during proton irradiation was observed, we concluded that the temperature was below the sensitization threshold to protons. Consequently, the sensitization in the presence of an acoustic modulation field was studied. Acoustic recordings with and without acoustic modulation and proton irradiation were performed at different temperatures, during cooling down of the water tank.

E. Ultrasound Sequence

The acoustic modulation and ultrasound imaging sequences are depicted in Fig. 2(a). Interferences between the modulation field and the monitoring sequences were avoided during the experiments by introducing a delay between the imaging sequence and modulation pulse. The acoustic modulation transducer was triggered by the Vantage system 40 μs after each image acquisition with the L12-5 array (8.9 MHz, plane waves, 0° angle). The pulse repetition frequency (PRF) for a single sequence (modulation + imaging) was 800 Hz. Effectively, each acquired image showed the effect of the previous modulation pulse. Long pulses (910 μs) at 1.1 MHz were used for acoustic modulation, achieving a 72% duty cycle. This high duty cycle ensured a higher number of proton-droplet interactions during the rarefactional phases of the acoustic modulation wave, which accounted for 36% of the total time. Each acquisition consisted of ten different acoustic pressures subsequently applied to the dilution of flowing droplets. 200 pulses were sent for each pressure step, from 0- to 900-kPa PNP, leading to a total acquisition time of 2.5 s. The irradiation always started before the ultrasound acquisition sequence and stopped once the acquisition was finished, providing a continuous proton beam during the whole sequence. After each acquisition, the cellulose tube was monitored, allowing the liquid flow to clear the produced bubbles before the next acquisition. For each temperature, three acquisitions were performed: 1) proton irradiation, no acoustic modulation; 2) proton irradiation and simultaneous acoustic modulation; and 3) acoustic modulation alone, without proton irradiation.

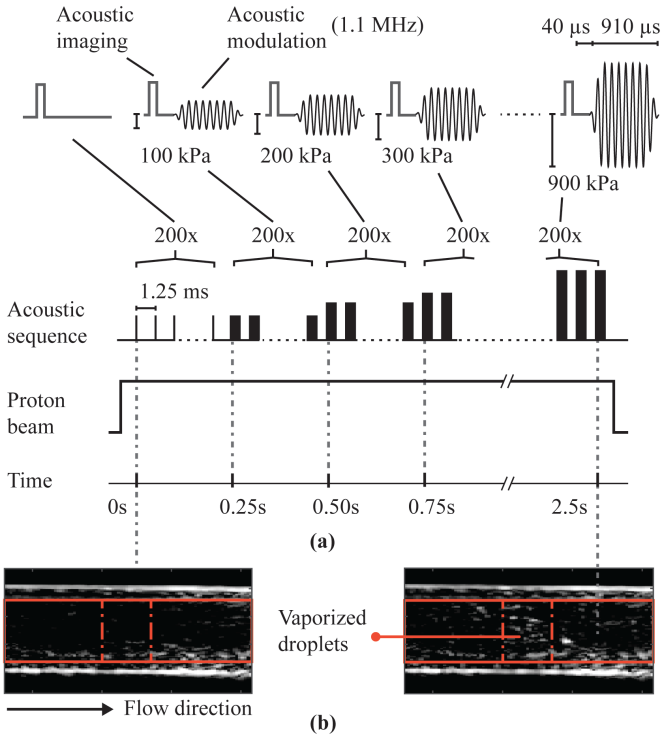

Fig. 2. (a) Timeline of the acoustic modulation experiments. (b) Example of a B-mode image of the tube at the start (left) and end (right) of an acquisition. The red solid lines represent the ROI, and the red dashed-dotted lines represent the −6-dB limit of the acoustic modulation beam. The bright spots at the center of the tube are vaporized NDs.

F. Data Processing

The radio frequency data recorded with the Vantage system was stored to a disk and processed offline. First, B-mode images were reconstructed using the built-in Verasonics beamformer (see Fig. 2(b)). Then, two regions of interest (ROI) were defined, one comprising the intersection of the proton beam cross section and the tube, and the other marking the

−6-dB limits of the acoustic modulation field. The boundaries of the first ROI were marked as the high vaporization density area on ultrasound recordings at 50 °C during proton irradiation. In order to determine the boundaries of the second ROI, the focus of the modulation field within the B-mode images was located using an acquisition in which the delay between the acoustic modulation and imaging pulses was removed. In this acquisition, the acoustic modulation field led to a change in the medium acoustic impedance which increased the backscatter intensity. The weighted centroids of the bright regions were used to locate the focus position in the lateral direction (see Fig. S3), and the −6-dB width measured with the hydrophone was then added.

Vaporization events in the ROI were measured and localized using the same principles as in [46]. Briefly, the frames were zero-phase filtered in slow time using a Butterworth high-pass filter (order 10, 300-Hz cut-off frequency, 25% pass-bandwidth). This step aimed at removing the slow changes in intensity between frames, only retaining the fast changes due to ND vaporization. Then, any image region whose intensity exceeded a given threshold, defined above the noise level in the frames without events, was localized and counted as a vaporization event. Finally, the vaporization counts were compared at different temperatures, in the presence and absence of acoustic modulation and proton irradiation.

III. Results

A. Sensitivity to Protons at Ambient Conditions

Fig. 3(a) shows the vaporization events distribution as a function of the lateral position in the tube and recording time for different relevant temperatures in the absence of acoustic modulation. We chose such representation—where the axial positions of the events inside the tube are stacked—to make more compact graphs, as the axial distribution of vaporization events was not relevant for this study. Each yellow dot represents an individual event. Since the beam cross section (13.3×13.3 mm^2 FWHM) covered most of the ROI defined in the ultrasound images (16×4 mm^2), the counts were distributed within the region of interest. The total number of counts (see Fig. 3(b)) was used as an indication of the sensitivity to protons at ambient conditions. The counts peaked at the highest investigated temperature (50 °C), and decreased with the temperature of the medium. This decreasing trend continued until the counts flattened below 43 °C. At this point, very few counts were measured (between 40 and 230 events during the 2.5-s recording), thus sensitivity to primary protons was assumed to be lost. Note that the 2-D spatial distributions of vaporization events for the entire temperature range are shown in Fig. S4.

B. Acoustically Modulated Sensitivity to Protons

When ND vaporization by protons was no longer observed at ambient conditions, the use of acoustic modulation to restore sensitivity to protons was investigated. The role of acoustic droplet vaporization (ADV) was also assessed during a second acquisition performed using the same acoustic modulation

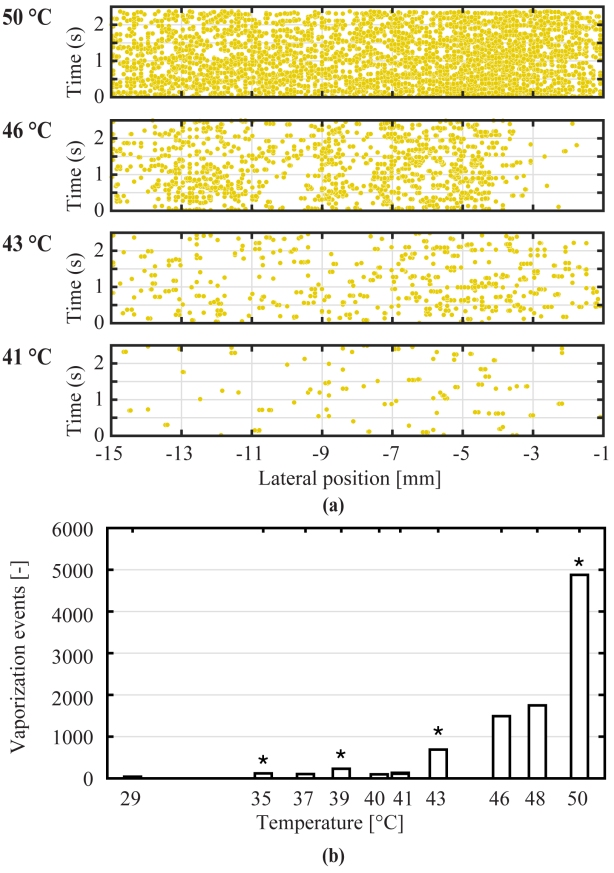

Fig. 3. (a) Vaporization maps during proton irradiation without acoustic modulation as a function of lateral position and time within the ROI for different temperatures. All axial positions within the ROI are included. (b) Total number of counts for recordings with proton irradiation only (no acoustic modulation) for all recorded temperatures. The stars indicate the temperatures at which the droplet solution was replenished.

sequence but without proton irradiation. Fig. 4 displays vaporization events again, but the vertical axis now represents the steps in acoustic modulation PNP. Each graph shows the data for one temperature. Supplementary data show the full 2-D spatial distribution of vaporization events in the tube for all pressure steps (see Fig. S5 and videos S6-10). Blue dots in Fig. 4 represent the vaporization events during proton irradiation with simultaneous acoustic modulation, while black dots represent the vaporization events for acoustic modulation alone (no irradiation). In the absence of acoustic modulation (0 kPa), the vaporization counts were negligible. A similar vaporization rate was observed until the PNP exceeded a certain threshold, which increased with decreasing temperatures. At low PNP, vaporization started at the acoustic modulation focus, represented by the two red dashed lines in Fig. 4. A further increase in modulation pressure amplitude resulted in a larger area where vaporization occurred. For all tested temperatures, the pressure at which vaporization occurred when the acoustic field was applied during proton irradiation was much lower than when the acoustic field was used alone (more than 500 kPa lower at the temperatures at which ADV was observed), thus showing a pressure range

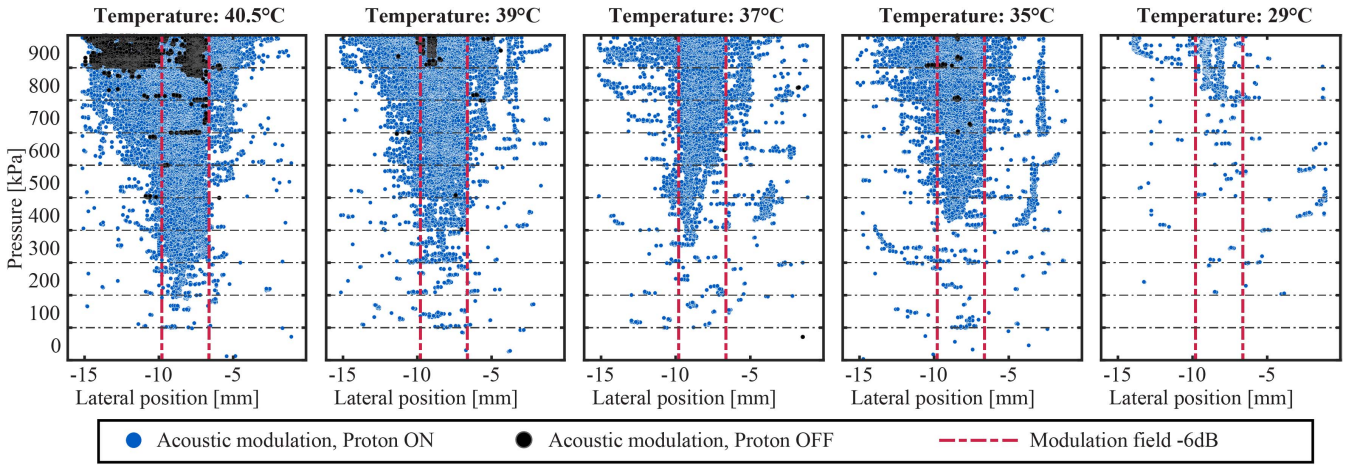

Fig. 4. Vaporization maps within the region of interest as a function of lateral position and acoustic pressure for different temperatures at which the droplets were not initially sensitive to protons. All axial positions within the ROI are included. The blue dots represent the counts during simultaneous proton irradiation and acoustic modulation, whereas the black dots correspond to acquisitions without proton irradiation (pure ADV due to the modulation field).

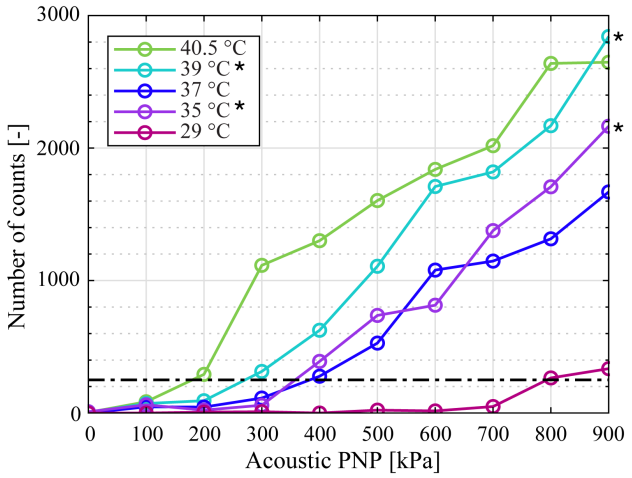

Fig. 5. Number of vaporization events during simultaneous proton irradiation and acoustic modulation after completing each pressure step for different temperatures. The horizontal dashed-dotted line represents the sensitization threshold defined as 250 events. Note that the acoustic PNP was increased by discrete steps of 100 kPa; the lines between individual points only aim at guiding the eye. The stars indicate the temperatures at which the droplet solution was replenished.

where vaporization events were induced by the combination of acoustic modulation and proton irradiation.

The number of counts at each pressure step is shown in Fig. 5. A threshold at 250 counts was used to estimate the sensitization pressure. Near this threshold value, an increase in the slope of the count curves can be observed for all temperatures, and after the threshold, the counts increased at each pressure step. In addition, the counts at each pressure decreased with temperature, except for 35 °C. Note that the NDs solution was replenished just before the acquisition at this temperature. The PNP threshold varied between 200 kPa at 40.5 °C and 800 kPa at 29 °C, with 400 kPa at 37 °C.

IV. Discussion

In this study, we have investigated the use of an acoustic modulation field to lower the radiation-induced vaporization threshold of PFB-NDs, in order to achieve direct sensitivity to protons. At ambient pressure (1.36 bar in our experiment), proton-induced vaporization events were observed at elevated temperatures (50 °C) and their number gradually decreased with temperature, until sensitivity to protons was lost between 43 °C and 41 °C. These observations are in agreement with previous findings for superheated drop detectors, which showed a smooth, sigmoidal sensitization to charged particles, rather than a steep change in vaporization count [14], [31]. We attribute the few residual vaporization counts observed for irradiations at temperatures below 41 °C to vaporizations due to high LET secondary particles and/or spontaneous vaporizations. A low-frequency acoustic field was then applied during proton irradiation, enabling proton-induced vaporization at acoustic PNPs ranging from 200 kPa (40.5 °C) to 800 kPa (29 °C), well below the ADV threshold found in this study ($>$800 kPa at 41 °C and lower temperatures). The use of an acoustic modulation field thus sensitized the NDs to protons at temperatures for which, at ambient pressure, such NDs would be vaporized by higher LET secondaries only [12].

While the energy sources differ, these observations are similar to findings reported for sono-photoacoustics, where ND vaporization was facilitated by the combination of laser heating of NDs coated with a plasmonic absorber and the rarefactional pressure from an acoustic wave [39], [40]. We hypothesize that a transient increase in the ND degree of superheat due to a pressure decrease during the rarefactional phases of the pulse was the mechanism leading to proton sensitization. Thermal heating due to ultrasound was estimated to be $<$0.01 °C during an acquisition, and therefore, was assumed to be negligible. During the rarefactional phase of an acoustic wave, the LET threshold decreases compared to

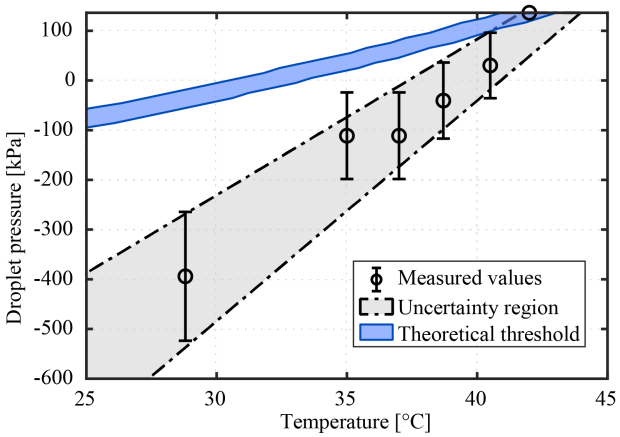

Fig. 6. Vaporization LET threshold as a function of temperature and pressure inside the droplet. The blue region represents the theoretical sensitization curve assuming a quasi-static effect of the acoustic pressure. The black markers are the values obtained experimentally, including the uncertainty associated with the 100-kPa pressure steps and hydrophone measurement.

its value at ambient conditions, and could thus reach values below the maximum LET of protons, allowing the latter to vaporize NDs.

The thermal spike theory equation (1) accurately predicted the sensitization threshold of superheated detectors when the ambient temperature or pressure changed in quasi-static conditions [32]. Thus, it is interesting to compare the theory with the experimental values we observed using an acoustic modulation field. Fig. 6 shows the theoretical sensitization threshold to protons represented as a blue region, in contrast to the experimental values, shown as black markers. In order to calculate the theoretical values, first, the experimental proton sensitization threshold at ambient pressure (1.36 bar, Fig. 3(b)) was used to estimate the nucleation parameter a. Combining the theoretical peak proton LET in PFB (74.5 keV/μm [47]) with the sensitization temperature observed experimentally (between 41 °C and 43 °C), we found an upper and lower limit for the nucleation parameter of 3.4 and 2.9, close to values previously reported in the literature for protons (i.e., $a = 2.1$–2.9) [10], [34]. Then, the theoretical LET threshold was determined as a function of temperature and pressure in the droplet core, assuming that the acoustic pressure adds quasi-statically to the ambient pressure. For the experimental values, the rms pressure (reached during 50% of the rarefactional phase) was used to take into account the oscillatory behavior of the wave, and uncertainties of $\pm$50 kPa (due to the pressure steps) and $\pm$15% (due to the hydrophone calibration) were added to the experimental points to form the uncertainty region from linear fits of the upper and lower limits. The experimentally determined acoustic pressures required for proton sensitization exceed the values predicted by the thermal spike theory, and the mismatch increases as the temperature decreases. In all cases, the differences are larger than the estimated uncertainties.

The discrepancy between theory and experiments could be due to limitations both in the theoretical model and in the method used in this study. The thermal spike model used to estimate the effect of the acoustic modulation field is static, neglecting dynamic effects, such as the radial oscillations that the acoustic modulation wave induces to a vapor embryo. These could result in shrinkage and disappearance of the embryo during the consecutive compressional phase [44], [48]. Such an effect would be highly frequency-dependent and would raise the acoustic pressure needed for vaporization, in comparison to a static change in ambient pressure assumed by the model. Moreover, the thermal spike model was shown to deviate from experimental observations, especially at low degrees of superheat [14], [32]. Finally, the model does neither account for the additional energy required to expand the viscoelastic shell during vaporization, nor for the effect of the Laplace pressure, both of which might be size-dependent. Modeling these effects requires a precise knowledge of the shell properties, such as the thickness, shear modulus, and viscosity at high strain rates, and lies outside of the scope of this work.

The method employed to find the sensitization thresholds reported in this study was based on the vaporization counts. Importantly, three conditions are required for the counting method to accurately quantify the number of vaporization events: vaporizations are sparse; microbubbles do not subsequently disappear; and flowing bubbles do not enter or leave the imaging plane. Due to limitations of the experimental setup used in our study, these conditions could not be entirely satisfied, as a large density of vaporization events was observed at high pressures, and some of the resulting microbubbles flowed in and out of the ultrasound field of view, likely resulting in an overestimation of vaporization events. However, we do not expect these limitations to significantly affect the sensitization threshold detection, as it is associated with low vaporization counts. A threshold corresponding to 250 vaporization counts was chosen as it qualitatively matches with a change in the slope of the count curves (see Fig. 5). The number of vaporization counts depends on the probability for a droplet to be simultaneously exposed to the PNP of the modulation wave and traversed by a proton at the end of its range. Spatially, the calibrated PNPs are only reached in a confined spot, and the effective width of the acoustic sensitization region grows together with the applied pressure, increasing the vaporization probability. This is observed in Fig. 4, as initially the vaporization region was confined to a small area near the transducer focus, and increased with the applied acoustic pressure. Temporally, the vaporization probability increases with the effective time during which the rarefactional pressure is lower than the sensitization threshold. Once the proton sensitization threshold is reached, the proton-induced vaporization probability also increases with the degree of superheat [14], [31]. For these three reasons (spatial uniformity of the pressure field, temporal variation of the pressure, and effect of the degree of superheat), the number of vaporization events are expected to increase with increasing PNP above the sensitization threshold. This might have led to an overestimation in the reported sensitization threshold values.

Additionally, it has been previously reported that the presence of microbubbles can reduce the acoustic vaporization threshold of superheated droplets, presumably owing to inertial cavitation of the microbubbles [49]. Given that some of the

vaporized NDs remained in the acoustic field during one acquisition, this effect might have impacted our measurements. However, we do not expect it to be the main mechanism, as we did not observe an avalanche of vaporizations when bubbles were seeded in the presence of a high intensity acoustic field. Instead, videos S6-10 show that when acoustic modulation is added to proton irradiation, vaporization events are distributed over a broad region. Besides, during control measurements with acoustic modulation in the absence of irradiation (black dots in Fig. 4 and Fig. S5), some sparse events were detected, which would also have led to an avalanche of vaporizations if a reduction in the ADV threshold due to the presence of microbubbles was the main mechanism.

Furthermore, the droplet concentration was not accurately controlled during all the acquisitions. The droplet dilution in the syringe was only renewed every 20–30 min, before the measurements at 50 °C, 43 °C, 39 °C, and 35 °C. Therefore, a concentration decrease over time might have occurred for measurements acquired in-between those temperatures. The latter can be clearly observed in Fig. 3(b), as lower counts than expected were observed for the temperatures at which the sample was not fresh. This decrease might have introduced a bias in the detection of the sensitization threshold in Fig. 5, as the 250 counts will be reached earlier if the concentration is higher. However, we do not expect it to have played a critical role, as large pressure steps were used in these experiments, and a consistent trend can be observed in the experimental sensitization threshold in Fig. 6.

All in all, taking the previous points into account, we suggest the reader to interpret the sensitization thresholds in this manuscript as a trend rather than an accurate assessment of the required acoustic pressure for proton sensitization. While this study shows the feasibility of modulating the NDs degree of superheat with a focused acoustic pressure field, the precise proton sensitization threshold should be determined in future studies. Ideally, a spatially uniform modulation field would be used, and longer recordings should be acquired for each modulation PNP, allowing a relevant statistical analysis and preventing the need to define an arbitrary value (e.g., 250 vaporization event counts) to determine the sensitization threshold. Furthermore, to unveil the physical mechanism, the influence of a series of important parameters, such as the acoustic modulation frequency, droplet size, droplet concentration, and droplet shell should be investigated in future studies.

The PNPs necessary for ADV were much higher than the PNPs necessary for proton sensitization at all investigated temperatures, as seen in Fig. 4. In recordings made using acoustic modulation alone, ADV was mostly observed at 40.5 °C for PNPs above 800 kPa, while only very few vaporization events were recorded for lower temperatures within the investigated PNPs (0–900 kPa). A wide range of ADV thresholds have been reported in the literature for PFB-NDs, ranging from 1.2 to 3.5 MPa at 37 °C [27], [50]–[53]. Such a large variation reflects the dependence of the ADV threshold on the ambient conditions, the acoustic pulse, and the droplet size, composition, and concentration. A recent study investigated the effect of most of these parameters on the ADV threshold of PFB-NDs, showing that it decreases with increasing pulse-length, PRF, temperature, droplet size and concentration, and with decreasing frequency [53]. Our study employed long pulses (1000 cycles), high PRF (800 Hz), and a relatively high droplet concentration (60–700 μM), together with a low US frequency (1.1 MHz), which could explain the relatively low pressure (800 kPa) at which the onset of ADV was observed at 40.5 °C.

We envision that acoustic modulation could enable proton-induced vaporization of PFB-NDs for *in vivo* range verification and dosimetry. Although indirect ND vaporization induced by secondary particles at physiological temperature could be used [11], [12], such an approach suffers from severe constraints. The presented technique allows direct proton detection while employing the popular PFB liquid as the ND core. In this study, we have used relatively large (∼800 nm) PVA-coated droplets compared to recent superheated ND studies (∼100–300 nm) [53]–[55]. However, although the sensitization threshold might be formulation dependent, we expect the acoustic modulation concept to apply to other droplet formulations and sizes. The droplet size is likely to have an impact on the clinical translation of this technique; smaller droplets might more easily extravasate from the leaky vasculature of tumors [56], which could potentially result in a more spatially homogeneous droplet distribution. On the other hand, the larger the droplet, the higher the probability of interaction with a proton, resulting in a larger number of vaporizations for the same number concentration. The optimal size for *in vivo* translation should be addressed in future studies.

The threshold PNP for proton-induced ND vaporization at 37 °C was as low as 400 kPa, which means that proton sensitization could be achieved *in vivo* with a mechanical index of 0.29. This value is well below the MI = 1.9 limit of FDA for diagnostic imaging [57] and is close to the values used in low-MI contrast-enhanced ultrasound (0.1–0.25 [58]–[60]). Since the Bragg peak in the proton direction is a few millimeters, and range shifts are expected to be in the order of millimeters, using a volumetric ultrasound system to sonicate a volume of $20 \times 20 \times 20$ mm^3 would enable range verification. While the achievable pressure uniformity over such an acoustic volume remains to be investigated *in vivo*, we do not expect non-uniformities to impede range verification, as long as the pressure remains sufficiently high to ensure sensitivity to protons in the entire acoustic volume. Ideally, the ultrasound array could be used both for acoustic modulation and imaging, reducing the setup complexity. In the present proof-of-concept study, a continuous proton beam was used together with an acoustic modulation field with a long pulse length and a high PRF (1000 cycles, 800 Hz), to increase the duty cycle, and hence the effective time during which NDs were simultaneously exposed to protons and ultrasound. These long pulses did not lead to a temperature increase in water during this experiment. However, tissue heating should be prevented in physiological applications and might limit the acoustic duty cycle. This can potentially compromise the performance for continuous proton beams, as the number of vaporization events will be directly related to the duty cycle. Therefore, although the acoustic modulation approach is feasible for all proton therapy

systems, in our opinion, the optimal clinical translation would be achieved for proton accelerators delivering a pulsed proton beam. In such a scenario, acoustic modulation can be applied for the duration of the proton spill, allowing a short pulse length and low duty cycle, while using the time in between proton bursts to image and localize ND vaporization events.

V. Conclusion

This manuscript reports on the feasibility of achieving direct vaporization of PFB-NDs by protons at physiological temperature by combining proton irradiation with a dynamic pressure modulation using an acoustic field. PVA-PFB NDs flowing in a tube were simultaneously irradiated with a proton beam and sonicated with acoustic waves of increasing pressure amplitudes, while ND vaporization was monitored by an ultrasound array positioned parallel to the tube. Proton-induced ND vaporization was observed at temperatures below the sensitization temperature corresponding to ambient pressure conditions and using acoustic pressures below the ADV threshold. We attribute this effect to an increase of the NDs degree of superheat during the rarefactional phase of the ultrasound wave, hence lowering the radiation-induced vaporization threshold. Importantly, the required PNP at 37 °C for proton sensitization was low (400 kPa), which suggests that acoustic modulation could be implemented clinically to enable *in vivo* proton range verification and dosimetry with the popular PFB-NDs.

Acknowledgment

The authors would like to thank Dr. Verya Daeichin for stimulating discussions and support, Dr. Yosra Toumia and Prof. Gaio Paradossi (University of Rome "Tor Vergata," Rome, Italy) for their support regarding the nanodroplet formulation, and Bram Carlier (KU Leuven, Leuven, Belgium) for technical discussions. They would also like to thank A. A. Brouwer (Erasmus MC, Rotterdam, The Netherlands), R. Beurskens (Erasmus MC), and H. den Bok (TU Delft, Delft, The Netherlands) for their help in designing and building the experimental apparatus.

References

[1] C. Grau, M. Durante, D. Georg, J. A. Langendijk, and D. C. Weber, "Particle therapy in Europe," *Mol. Oncol.*, vol. 14, no. 7, pp. 1492–1499, Jul. 2020.

[2] K. Parodi and J. C. Polf, "*In vivo* range verification in particle therapy," *Med. Phys.*, vol. 45, no. 11, pp. e1036–e1050, Nov. 2018.

[3] H. Paganetti, *Proton Therapy Physics*. Boca Raton, FL, USA: CRC Press, 2019.

[4] H. Paganetti, "Range uncertainties in proton therapy and the role of Monte Carlo simulations," *Phys. Med. Biol.*, vol. 57, no. 11, pp. R99–R117, Jun. 2012.

[5] A. C. Knopf and A. Lomax, "*In vivo* proton range verification: A review," *Phys. Med. Biol.*, vol. 58, no. 15, pp. 131–160, 2013.

[6] J. C. Polf and K. Parodi, "Imaging particle beams for cancer treatment," *Phys. Today*, vol. 68, no. 10, pp. 28–33, Oct. 2015.

[7] F. Seitz, "On the theory of the bubble chamber," *Phys. Fluids*, vol. 1, no. 1, pp. 2–13, 1958.

[8] D. A. Glaser, "Bubble chamber tracks of penetrating cosmic-ray particles," *Phys. Rev.*, vol. 91, no. 3, pp. 762–763, Aug. 1953.

[9] R. E. Apfel, "The superheated drop detector," *Nucl. Instrum. Methods*, vol. 162, nos. 1–3, pp. 603–608, Jun. 1979.

[10] F. d'Errico, "Radiation dosimetry and spectrometry with superheated emulsions," *Nucl. Instrum. Methods Phys. Res. B, Beam Interact. Mater. At.*, vol. 184, nos. 1–2, pp. 229–254, 2001.

[11] B. Carlier *et al.*, "Proton range verification with ultrasound imaging using injectable radiation sensitive nanodroplets: A feasibility study," *Phys. Med. Biol.*, vol. 65, no. 6, Mar. 2020, Art. no. 065013.

[12] S. V. Heymans *et al.*, "Modulating ultrasound contrast generation from injectable nanodroplets for proton range verification by varying the degree of superheat," *Med. Phys.*, vol. 48, no. 4, pp. 1983–1995, Apr. 2021.

[13] G. Collado-Lara *et al.*, "Spatiotemporal distribution of nanodroplet vaporization in a proton beam using real-time ultrasound imaging for range verification," *Ultrasound Med. Biol.*, vol. 48, no. 1, pp. 149–156, Jan. 2022.

[14] F. d'Errico, "Fundamental properties of superheated drop (bubble) detectors," *Radiat. Protection Dosimetry*, vol. 84, nos. 1–4, pp. 55–62, 1999.

[15] H. Ing, R. A. Noulty, and T. D. McLean, "Bubble detectors—A maturing technology," *Radiat. Meas.*, vol. 27, no. 1, pp. 1–11, Feb. 1997.

[16] S. C. Roy, "Superheated liquid and its place in radiation physics," *Radiat. Phys. Chem.*, vol. 61, nos. 3–6, pp. 271–281, Jun. 2001.

[17] K. Parodi *et al.*, "Patient study of *in vivo* verification of beam delivery and range, using positron emission tomography and computed tomography imaging after proton therapy," *Int. J. Radiat. Oncol. Biol. Phys.*, vol. 68, no. 3, pp. 920–934, Jul. 2007.

[18] C. H. Min *et al.*, "Clinical application of in-room PET for *in vivo* treatment monitoring in proton radiotherapy," *Int. J. Radiat. Oncol. Biol. Phys.*, vol. 86, no. 1, pp. 183–189, 2013.

[19] A. C. Kraan *et al.*, "Proton range monitoring with in-beam PET: Monte Carlo activity predictions and comparison with cyclotron data," *Phys. Medica*, vol. 30, no. 5, pp. 559–569, Jul. 2014.

[20] C. Richter *et al.*, "First clinical application of a prompt gamma based *in vivo* proton range verification system," *Radiotherapy Oncol.*, vol. 118, no. 2, pp. 232–237, Feb. 2016.

[21] Y. Xie *et al.*, "Prompt gamma imaging for *in vivo* range verification of pencil beam scanning proton therapy," *Int. J. Radiat. Oncol. Biol. Phys.*, vol. 99, no. 1, pp. 210–218, Sep. 2017.

[22] Y. Jongen and F. Stichelbaut, "Verification of the proton beams position in the patient by the detection of prompt gamma-rays emission," in *Proc. 39th Meeting Part. Therapy Co-Operative Group*, Oct. 2003, pp. 1–16.

[23] M. Durante and H. Paganetti, "Nuclear physics in particle therapy: A review," *Rep. Prog. Phys.*, vol. 79, no. 9, Sep. 2016, Art. no. 096702.

[24] S. España, X. Zhu, J. Daartz, G. El Fakhri, T. Bortfeld, and H. Paganetti, "The reliability of proton-nuclear interaction cross-section data to predict proton-induced PET images in proton therapy," *Phys. Med. Biol.*, vol. 56, no. 9, pp. 2687–2698, May 2011.

[25] G. P. Biro, P. Blais, and A. L. Rosen, "Perfluorocarbon blood substitutes," *Crit. Rev. Oncol./Hematol.*, vol. 6, no. 4, pp. 311–374, Jan. 1987.

[26] P. S. Sheeran, J. D. Rojas, C. Puett, J. Hjelmquist, C. B. Arena, and P. A. Dayton, "Contrast-enhanced ultrasound imaging and *in vivo* circulatory kinetics with low-boiling-point nanoscale phase-change perfluorocarbon agents," *Ultrasound Med. Biol.*, vol. 41, no. 3, pp. 814–831, Mar. 2015.

[27] P. S. Sheeran, K. Yoo, R. Williams, M. Yin, F. S. Foster, and P. N. Burns, "More than bubbles: Creating phase-shift droplets from commercially available ultrasound contrast agents," *Ultrasound Med. Biol.*, vol. 43, no. 2, pp. 531–540, Feb. 2017.

[28] K. Yoo, W. R. Walker, R. Williams, C. Tremblay-Darveau, P. N. Burns, and P. S. Sheeran, "Impact of encapsulation on *in vitro* and *in vivo* performance of volatile nanoscale phase-shift perfluorocarbon droplets," *Ultrasound Med. Biol.*, vol. 44, no. 8, pp. 1836–1852, Aug. 2018.

[29] H. Lea-Banks, M. A. O'Reilly, C. Hamani, and K. Hynynen, "Localized anesthesia of a specific brain region using ultrasound-responsive barbiturate nanodroplets," *Theranostics*, vol. 10, no. 6, pp. 2849–2858, 2020.

[30] F. d'Errico, R. Nath, and R. Nolte, "A model for photon detection and dosimetry with superheated emulsions," *Med. Phys.*, vol. 27, no. 2, pp. 401–409, Feb. 2000.

[31] S. Archambault *et al.*, "New insights into particle detection with superheated liquids," *New J. Phys.*, vol. 13, no. 4, Apr. 2011, Art. no. 043006.

[32] H. R. Andrews *et al.*, "LET dependence of bubble detector response to heavy ions," *Radiat. Protection Dosimetry*, vol. 120, nos. 1–4, pp. 480–484, Sep. 2006.

[33] F. D'Errico and E. Egger, "Proton beam dosimetry with superheated drop (bubble) detectors," in *Hadrontherapy in Oncology* (Excerpta Medica International Congress Series), U. Amaldi and B. Larsson, Eds. Amsterdam, The Netherlands: Elsevier, 1994, pp. 488–494.

[34] A. R. Green *et al.*, "Bubble detector characterization for space radiation," *Acta Astronautica*, vol. 56, nos. 9–12, pp. 949–960, May 2005.

[35] M. A. Borden, G. Shakya, A. Upadhyay, and K.-H. Song, "Acoustic nanodrops for biomedical applications," *Current Opinion Colloid Interface Sci.*, vol. 50, Dec. 2020, Art. no. 101383.

[36] P. A. Mountford and M. A. Borden, "On the thermodynamics and kinetics of superheated fluorocarbon phase-change agents," *Adv. Colloid Interface Sci.*, vol. 237, pp. 15–27, Nov. 2016.

[37] P. A. Mountford, A. N. Thomas, and M. A. Borden, "Thermal activation of superheated lipid-coated perfluorocarbon drops," *Langmuir*, vol. 31, no. 16, pp. 4627–4634, Apr. 2015.

[38] P. S. Sheeran *et al.*, "Methods of generating submicrometer phase-shift perfluorocarbon droplets for applications in medical ultrasonography," *IEEE Trans. Ultrason., Ferroelectr., Freq. Control*, vol. 64, no. 1, pp. 252–263, Jan. 2017.

[39] B. Arnal *et al.*, "Sono-photoacoustic imaging of gold nanoemulsions: Part I. Exposure thresholds," *Photoacoustics*, vol. 3, no. 1, pp. 3–10, Mar. 2015.

[40] B. Arnal *et al.*, "Sono-photoacoustic imaging of gold nanoemulsions: Part II. Real time imaging," *Photoacoustics*, vol. 3, no. 1, pp. 11–19, Mar. 2015.

[41] D. S. Li, G.-S. Jeng, J. J. Pitre, M. Kim, L. D. Pozzo, and M. O'Donnell, "Spatially localized sono-photoacoustic activation of phase-change contrast agents," *Photoacoustics*, vol. 20, Dec. 2020, Art. no. 100202.

[42] Y. Toumia *et al.*, "Ultrasound-assisted investigation of photon triggered vaporization of poly(vinylalcohol) phase-change nanodroplets: A preliminary concept study with dosimetry perspective," *Phys. Medica*, vol. 89, pp. 232–242, Sep. 2021.

[43] G. Lajoinie, T. Segers, and M. Versluis, "High-frequency acoustic droplet vaporization is initiated by resonance," *Phys. Rev. Lett.*, vol. 126, no. 3, Jan. 2021, Art. no. 034501.

[44] O. Shpak, O. Verweijx, H. J. Vos, N. de Jong, D. Lohse, and M. Versluis, "Acoustic droplet vaporization is initiated by superharmonic focusing," *Proc. Nat. Acad. Sci. USA*, vol. 111, no. 5, pp. 1697–1702, Feb. 2014.

[45] W. D. Newhauser and R. Zhang, "The physics of proton therapy," *Phys. Med. Biol.*, vol. 60, no. 8, pp. R155–R209, 2015.

[46] C. Errico *et al.*, "Ultrafast ultrasound localization microscopy for deep super-resolution vascular imaging," *Nature*, vol. 527, no. 7579, pp. 499–502, Nov. 2015.

[47] J. E. Turner, *Atoms, Radiation, and Radiation Protection*, 3rd ed. Weinheim, Germany: Wiley, 2007.

[48] T. Lacour, M. Guédra, T. Valier-Brasier, and F. Coulouvrat, "A model for acoustic vaporization dynamics of a bubble/droplet system encapsulated within a hyperelastic shell," *J. Acoust. Soc. Amer.*, vol. 143, no. 1, pp. 23–37, Jan. 2018.

[49] A. H. Lo, O. D. Kripfgans, P. L. Carson, E. D. Rothman, and J. B. Fowlkes, "Acoustic droplet vaporization threshold: Effects of pulse duration and contrast agent," *IEEE Trans. Ultrason., Ferroelectr., Freq. Control*, vol. 54, no. 5, pp. 933–946, May 2007.

[50] C. de Gracia Lux *et al.*, "Novel method for the formation of monodisperse superheated perfluorocarbon nanodroplets as activatable ultrasound contrast agents," *RSC Adv.*, vol. 7, no. 77, pp. 48561–48568, 2017.

[51] D. S. Li, S. Schneewind, M. Bruce, Z. Khaing, M. O'Donnell, and L. Pozzo, "Spontaneous nucleation of stable perfluorocarbon emulsions for ultrasound contrast agents," *Nano Lett.*, vol. 19, no. 1, pp. 173–181, Jan. 2019.

[52] J. D. Rojas, M. A. Borden, and P. A. Dayton, "Effect of hydrostatic pressure, boundary constraints and viscosity on the vaporization threshold of low-boiling-point phase-change contrast agents," *Ultrasound Med. Biol.*, vol. 45, no. 4, pp. 968–979, Apr. 2019.

[53] Q. Wu *et al.*, "Investigation of the acoustic vaporization threshold of lipid-coated perfluorobutane nanodroplets using both high-speed optical imaging and acoustic methods," *Ultrasound Med. Biol.*, vol. 47, no. 7, pp. 1826–1843, Jul. 2021.

[54] G. Zhang *et al.*, "Acoustic wave sparsely activated localization microscopy (AWSALM): Super-resolution ultrasound imaging using acoustic activation and deactivation of nanodroplets," *Appl. Phys. Lett.*, vol. 113, no. 1, Jul. 2018, Art. no. 014101.

[55] B. L. Helfield *et al.*, "Investigating the accumulation of submicron phase-change droplets in tumors," *Ultrasound Med. Biol.*, vol. 46, no. 10, pp. 2861–2870, Oct. 2020.

[56] K. Kooiman *et al.*, "Ultrasound-responsive cavitation nuclei for therapy and drug delivery," *Ultrasound Med. Biol.*, vol. 46, no. 6, pp. 1296–1325, Jun. 2020.

[57] S. B. Barnett, G. R. T. Haar, M. C. Ziskin, H.-D. Rott, F. A. Duck, and K. Maeda, "International recommendations and guidelines for the safe use of diagnostic ultrasound in medicine," *Ultrasound Med. Biol.*, vol. 26, no. 3, pp. 355–366, Mar. 2000.

[58] T. K. Kim, H.-J. Jang, P. N. Burns, J. Murphy-Lavallee, and S. R. Wilson, "Focal nodular hyperplasia and hepatic adenoma: Differentiation with low-mechanical-index contrast-enhanced sonography," *Amer. J. Roentgenol.*, vol. 190, no. 1, pp. 58–66, Jan. 2008.

[59] C. F. Dietrich, A. Ignee, and H. Frey, "Contrast-enhanced endoscopic ultrasound with low mechanical index: A new technique," *Zeitschrift für Gastroenterologie*, vol. 43, no. 11, pp. 1219–1223, Nov. 2005.

[60] H.-X. Xu *et al.*, "Imaging of peripheral cholangiocarcinoma with low-mechanical index contrast-enhanced sonography and SonoVue," *J. Ultrasound Med.*, vol. 25, no. 1, pp. 23–33, Jan. 2006.

Sophie V. Heymans (Student Member, IEEE) was born in Namur, Belgium, in 1992. She received the M.Sc. degree in electromechanical engineering from the Université Catholique de Louvain, Louvain-la-Neuve, Belgium, in 2014, the M.Sc. degree in biomedical engineering from Imperial College London, London, U.K., in 2015, and the joint Ph.D. degree from KU Leuven, Leuven, Belgium, and Erasmus University Rotterdam, Rotterdam, The Netherlands, in 2022.

From 2015 until 2018, she worked as a Research and Development Physicist with Ion Beam Applications, Ottignies-Leuven-la-Neuve. She was a Research Assistant with KU Leuven, and the Erasmus Medical Center, Rotterdam, from 2018 to 2022. She is currently a Postdoctoral Research Associate with KU Leuven. Her research interests include the use of ultrasound contrast agents for the monitoring of radiotherapy and proton therapy, ultrafast imaging, and super-resolution ultrasound imaging.

Dr. Heymans was awarded the Ash Prize for the Best Academic Performance in the M.Sc. Program and the IPEM Prize for the Best M.Sc. Project in medical physics in 2015.

Gonzalo Collado-Lara received the B.S. and M.S. degrees in aerospace engineering from the University of Seville, Seville, Spain, in 2015 and 2017, respectively. He is currently pursuing the Ph.D. degree in biomedical engineering with the Erasmus Medical Center, Rotterdam, The Netherlands.

In 2018, he was a Prototype Developer with Bracco Suisse SA, Geneva, Switzerland. The main topic of his research interest includes ultrasound contrast agents for dosimetry in radiotherapy. His research interests also include the production of the contrast agents, to cavitation phenomena and super-localization.

Marta Rovituso received the Ph.D. degree from the GSI Helmholtz Center for Heavy Ion Research, Technical University of Darmstadt, Darmstadt, Germany, in 2016, focusing on the physical characterization of Helium ions for application in cancer treatments, especially for pediatric patients.

From 2016 to 2019, she was a Postdoctoral Research Associate with the Italian Institute of Nuclear Physics, Trento, Italy. In 2019, she was appointed as a Beam Line Scientist of the Holland Proton Therapy Center, Delft, The Netherlands. Her research interests include advanced beam line technologies to perform radiobiological experiments, which go from cell to animal irradiations, physics, dosimetry, and space applications.

Dr. Rovituso was a recipient of the Christoph Schmelzer Award in 2016.

Hendrik J. Vos (Member, IEEE) received the M.Sc. degree in applied physics from the Delft University of Technology, Delft, The Netherlands, in 2004, and the Ph.D. degree from the Department of Biomedical Engineering, Erasmus University Medical Center (Erasmus MC), Rotterdam, The Netherlands, in 2010.

He worked as a Postmaster Researcher with the University of Florence, Florence, Italy, and a Contract Researcher of the petrochemical industry on cutting-edge ultrasonic solutions. He is currently an Associate Professor with the Erasmus MC and the Delft University of Technology. His research interests include acoustical array technology for biomedical imaging in all its aspects: transducers, 2-D and 3-D beamforming, cardiac shear waves, ultrafast Doppler, contrast imaging, and related subclinical and clinical studies.

Dr. Vos received a Dutch NWO-TTW-VIDI Personal Grant in 2018.

Jan D'hooge (Member, IEEE) was born in Sint-Niklaas, Belgium, in 1972. He received the M.Sc. and Ph.D. degrees in physics from the University of Leuven, Leuven, Belgium, in 1994 and 1999, respectively.

He was a Postdoctoral Researcher with the Medical Imaging Computing Laboratory, Department of Electrical Engineering, University of Leuven, where he became acquainted with general problems in medical imaging, such as elastic registration, segmentation, shape analysis, and data acquisition problems related to other modalities (in particular, MRI). In 2006, he was appointed as an Associate Professor with the Department of Cardiovascular Sciences, Faculty of Medical, University of Leuven. From 2009 till 2021, he has been a part-time Visiting Researcher with the Norwegian Institute of Science and Technology, Trondheim, Norway, and is, since 2020, an Honorary Affiliate of the Institute of Cardiovascular Science, University College London, London, U.K. He has authored or coauthored over 300 peer-reviewed articles, has contributed to 14 books, and has coedited two books. His current research interests include myocardial tissue characterization, deformation imaging, and cardiac pathophysiology.

Dr. D'hooge was an elected Ad Com Member of the IEEE-UFFC Society from 2010 to 2012. He is currently a member of the Acoustical Society of America and the European Association of Echocardiography. He was awarded a prestigious ERC Consolidator Grant; gave the 2018 Kalmanson Lecturer of the American Society of Echocardiography, and won the 2019 IEEE Ultrasonics Carl Hellmuth Hertz Award. He was the Chair of the Ultrasound Conference of the SPIE Medical Imaging Symposium from 2008 to 2011, the Technical Vice-Chair of the IEEE Ultrasonics Symposium from 2008 to 2012, and its Technical Chair in 2014 and 2018. From 2019 till 2022, he was the Chair of the IEEE Ultrasonics Symposium Guidance Committee. In August 2021, he was appointed as a Vice-Rector on research policy of KU Leuven.

Nico de Jong (Member, IEEE) received the M.Sc. degree in physics with a specialized in pattern recognition from the Delft University of Technology, Delft, The Netherlands, in 1978, and the Ph.D. degree in acoustic properties of ultrasound contrast agents from the Department of Biomedical Engineering, Thorax Center, Erasmus University Medical Center (Erasmus MC), Rotterdam, The Netherlands, in 1993.

Since 1980, he has been a Staff Member with the Thorax Center, Erasmus MC. Since 2011, he has been a Professor of molecular ultrasonic imaging and therapy with Erasmus MC and the Delft University of Technology, where he was the Head of the Medical Imaging Section until 2021. In 2003, he joined the University of Twente, Enschede, The Netherlands, as a part-time Professor. He currently teaches with technical universities and Erasmus MC. Over the last five years, he has given over 30 invited lectures and has given numerous scientific presentations for international industries. He has been a Principal Investigator (PI) and the work package leader of European and Dutch projects. He has authored 260 peer-reviewed articles.

Prof. de Jong is also the Organizer of the Annual European Symposium on Ultrasound Contrast Imaging, Rotterdam, which is attended by approximately 175 scientists from universities and industries all over the world. He is on the Safety Committee of the World Federation of Ultrasound in Medicine and Biology, an Associate Editor of Ultrasound in Medicine and Biology, and a Guest Editor of the special issues of different journals.

Koen Van Den Abeele was born in Lokeren, Belgium, in 1965. He received the M.Sc. degree in applied mathematics from KU Leuven, Leuven, Belgium, in 1987, and the Ph.D. degree in mathematical physics and applied mathematics from KU Leuven, in 1992, on the subject "Alternative Fundamental Theoretical Descriptions for Acousto-Optic and Acoustic Investigation of Pulsed and Profiled Ultrasound in View of Nondestructive Testing of Layered Structures."

He is currently a Full Professor with KU Leuven, the Head of the Wave Propagation and Signal Processing Research Group, KU Leuven at Kulak, Kortrijk, Belgium, and the Chair of the group Science Engineering and Technology, KU Leuven at Kulak. He has been continuously involved in EU projects since 2000 as a coordinator or a partner. He is the (co)author of more than 200 journal publications and conference proceedings. His research interests include theoretical modeling and experimental verification of linear and nonlinear wave propagation phenomena in liquid and solid media, and its application to nondestructive evaluation (NDE), damage detection, quality control in industrial materials, monitoring of bio(techno)logical processes, and ultrasound-based dosimetry.